

# Production and Characterization of Zr Based Bulk Metallic Glass Matrix Composites (BMGMC) in the Form of Wedge Shape Ingots

Muhammad Musaddique Ali Rafique

Eastern Engineering Solutions LLC, Detroit, MI, USA  
Email: ali.rafique@hotmail.com

**How to cite this paper:** Rafique, M.M.A. (2018) Production and Characterization of Zr Based Bulk Metallic Glass Matrix Composites (BMGMC) in the Form of Wedge Shape Ingots. *Engineering*, 10, 215-245. <https://doi.org/10.4236/eng.2018.104015>

**Received:** February 22, 2018  
**Accepted:** April 27, 2018  
**Published:** April 30, 2018

Copyright © 2018 by author and Scientific Research Publishing Inc. This work is licensed under the Creative Commons Attribution International License (CC BY 4.0).  
<http://creativecommons.org/licenses/by/4.0/>



Open Access

## Abstract

Bulk metallic glass matrix composites (BMGMC) are unique materials of future having excellent mechanical properties (such as high hardness, strength and profound elastic strain limit). However, they exhibit poor ductility and suffer from catastrophic failure on the application of force. The reasons behind this are still not very well understood. In this study, an effort has been made to overcome this pitfall by solidification processing. Zr based BMGMCs are produced in the form of “as cast” wedges using vacuum arc melting and suction casting button furnace. The idea is to study the effect of cooling rate and inoculation on formability during solidification. Adjustment, manipulation and proper control of processing parameters are observed to reflect upon the quality of ingots such as improved castability, proper mold filling and defect free casting as characterized by NDT. Further, thermal analysis, optical microscopy and hardness measurement confirmed the formation and evolution of *in-situ* composite structure. This is first footprint of pathway towards sustainable manufacturing of these alloys in future.

## Keywords

BMGMC, as Cast, Dendrite, Ingot, Toughness

## 1. Introduction

Bulk metallic glass matrix composites have attracted the attention of scientific community lately due to their unique and superior mechanical properties which include high hardness, associated high strength and very high elastic strain limit which make them suitable for applications which require shock energy absorp-

tion for a very short transient period of time (e.g. whipple shield of space shuttle [1], spacecraft shielding [2] and whipple shield of International Space Station (ISS) [1]-[7]). They are potential candidates for parts of high speed moving aero structures which may come in contact with high speed projectiles (such as meteors, space debris and reentry targets) and wear resistant surfaces both involving static (sliding surfaces [8] [9] [10] [11]) and dynamic (gears [12] [13]) load applications. Further, low density, high specific strength and excellent corrosion resistance in their Ti based versions make them a strong candidate for future aerospace applications [14] [15]. However, some of their variants have very poor glass forming ability (GFA) (Al based BMGMCs) and high brittleness (Mg based BMGMCs). Overall, due to presence of glassy structure which imparts strength and hardness, they also become brittle with exhibition of plasticity thus it is very difficult to make complex shape components from them [16] [17]. They undergo catastrophic failure in milliseconds by rapid movement of shear bands [18] [19] [20] which move at a high speed throughout volume of material in some cases producing heat [21]-[25]. Mainly, two mechanisms are proposed to counter this namely *ex-situ* [26] [27] or *in-situ* [28] [29] introduction of foreign objects/particles/precipitates during liquid state (solidification) or solid state (devitrification [30] [31]) processing. The strengthening mechanism by which this happens is corroborated to shear band pinning [32] [33] [34] [35], multiplication [36] [37] [38], size reduction [39] [40] [41], and precipitation hardening [42]-[47]. Various techniques have been proposed to achieve this such as powder processing [48] [49], fluxing [50] [51] [52], solid state processing [53], semi-solid processing [54], twin roll casting (TRC) [55] [56], thermoplastic forming (TPF) [57] [58], blow molding/forming [59] [60] and superplastic forming [61] which may serve the purpose of producing strong and tough material [62] [63] [64] but vacuum arc melting (VAM) and suction casting remains as the major method for most of production of these alloys in the world. It relies on melting a certain precursor of alloying elements in vacuum arc melting (VRM) furnace and then drawing molten melt in a water cooled Cu mold (length/diameter > 1) under the action of pressure difference causing a suction effect thus producing rod shape specimens. First successful study describing *in-situ* introduction of primary phase ductile precipitates nucleating in the form of three dimensional dendrites out of melt was reported by Prof. Johnson's group at Caltech in 2000 [28] in which they introduced B2 CuZr phase in Zr based BMGMC during solidification spread all across volume of specimen. This was a major discovery of that time. The largest rod reported till date by this method is 85 mm in length and 80 mm in diameter produced in the group of Prof. Inoue at WPI-IMR, Tohoko University, Japan [65]. Exact mechanism by which this happens is not well understood and there is dearth of knowledge about how second phase particles nucleate from melt during solidification. Various efforts covering both theoretical (modeling and simulation) and experimental fronts have been made to understand and describe the nucleation and growth pheno-

mena in these alloys during solidification. These include use of levitation (electrostatic levitation (ESL) [66] [67]/aerodynamic levitation (ADL)) experiments in Synchrotron light [68] [69] [70], micro and zero gravity solidification [5] and advanced modeling and simulation proprietary platforms COMSOL®, Ansys®, Dessault Systems (DSS) Solidworks®, ABAQUS®, ProCast® (ESI Group), Magma flow® and Flow3D® (LANL). However, no study has been carried out which includes the use of wedge shape castings with potent inoculants to study the effect of cooling rate and inoculation on microstructure evolution in BMGMCs. This study aims to bridge this gap. Series of experiments were carried out to cast small BMGMCs wedges from Cu mold suction casting after vacuum arc melting without and with varying percentages of inoculants. *First aim* was to determine the effectiveness of 1) “cooling rate” to assist the formation of glassy structure and 2) “potent inoculants” to help provide seed for nucleation in rapidly cast alloys. Both mechanisms are meant to be tailored to such an extent that BMGMCs with superior ductility can be manufactured detailing their effective ‘safe structural design limit’ for practical industrial applications. The *second aim* of study was to understand the volume which may contain fully vitrified structure (100% glass), partially vitrified glass [21] [43] [71], and no glass (100% crystallization) zones by virtue of measurement of volume fraction (number density ( $d_c$ )), size and distribution of ductile phase (B2 or  $\beta$ -Zr) in that particular region. Keeping alloying elements constant; amount, number density, size, distribution and type of ductile phase (grains) change with change of section thickness [72]. The same phenomenon is observed in liquid melt pool of additively manufactured components in various layers. Thus, this study is meant to provide a platform for developing production strategies for manufacturing of BMGMC components using Additive Manufacturing (AM). *Last but not least aim* was to determine the processing window of casting parameters which can ascertain a chemical composition for a certain dimension that yield superior casting properties (avoiding miss runs, improper filling, low fluidity, poor castability, super heat, porosity, laps, surface cracking and shrinkage).

## 2. Experimental—Manufacturing Procedure

Zr based bulk metallic glass matrix composites (BMGMC) are produced using vacuum arc melting (VRM) and Cu mold suction casting furnace. This is typical button furnace used to produce small casted ingots in the form of buttons using very small charge. It consists of a high pressure chamber which houses chilled water cooled Cu hearth and an electrode which is used to produce arc as a result of its contact (make and break) with strike piece at hearth for a very short period of time. Intensity of arc and hence temperature generated can be controlled by frequency of transformer unit at the back end. In principle, it is medium frequency welding transformer which is responsible for generation of arc. Construction of chamber consists of double wall jacketed body with circulating water in it which serves the purpose of heat sink. Heat generated from arcing at

hearth is extracted by circulating chilled water. A temperature sensor triggers a shutdown alarm and activates switch which disconnects power to furnace if water temperature goes beyond 8°C. Whole chamber can be lifted with the help of hydraulic jack connected to body via a manual ram. The furnace chamber body is also supplied with two viewing windows carrying high temperature infrared glass for observation inside chamber. This high temperature resistant opaque glass is free to slide in and out of small rectangular slot. This slot is also equipped with motion sensor which again shutdown the power to furnace if protecting glass is removed during the process or not at all inserted at initial stage. Both safety features enable protection of personal and surroundings and ensure smooth operation of furnace. Vacuum is caused by operation of small rotary vane pump connected to main melting chamber. It can generate a vacuum up to  $10^{-3}$  mbar. A gas port serves the purpose of injection of Argon to chamber when needed. Furnace is loaded with small charge into a horizontal slot in the hearth and is closed for rough vacuum. After evacuation, chamber is filled with Argon to remove any air in it. Oxygen in air tends to adsorb on Ar and is meant to be sucked away during next evacuation cycle. This evacuation and purging cycle is repeated six times to ensure near absolute vacuum. After last evacuation, chamber is filled with 12 mbar of Ar overpressure. Melting process is carried out under this overpressure as arc cannot be established and stabilized in absolute vacuum. After melting, which lasts for few minutes depending upon charge, ingot is sucked from top of oval shape chute to wedge shape Cu mold by instantaneous opening of bleeding valve connected with main evacuation line. This process lasts for very short time during which casting solidifies in mold cavity. Advantages of process include; it is very cheap process, raw material, running and maintenance costs are low, it is reproducible and clean process. Disadvantages are; its batch process, its time consuming (long pumping cycle), pumping process is not very efficient, limited by raw material type (mostly powder), mostly it is manual process with no automation and quality of casting varies with skill of operator. Process flow diagram of whole setup is schematically shown in **Figure 1**.

### 3. Results and Discussion

Physical, chemical and thermal analyses are performed on castings produced. These are described one by one as under.

#### 3.1. Visual Inspection

First of all, wedge shape castings are visually inspected for quality purpose. A general criterion defined in ASTM A802/A802M - 95/AS 3978 - 2003 is used for this purpose. Acceptance levels for surface texture, non-metallic inclusions, and gas porosity and solidification discontinuities are used. General visual inspection details as observed on different samples is depicted in figures (**Figures 2(a)-(f)**).

**Figure 2(a)** is picture of first casted wedge. It is  $Zr_{47.5}Cu_{45.5}Al_8Co_2$  alloy. As can

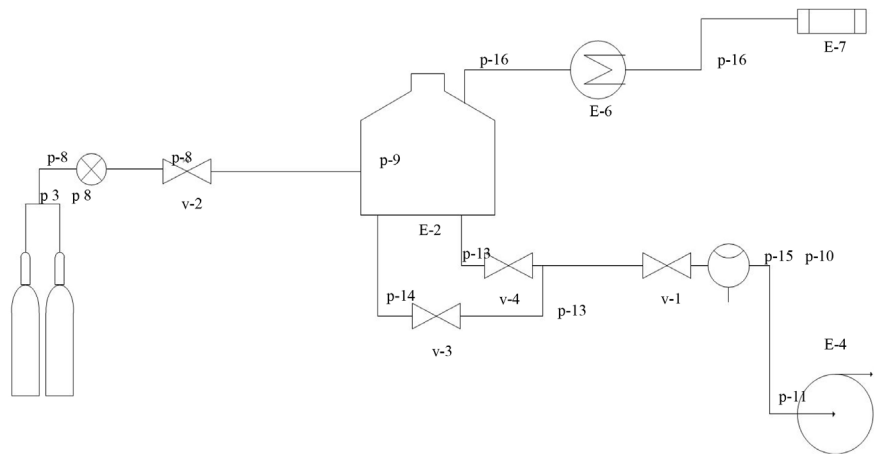


**Figure 1.** Schematic flow diagram of vacuum arc melting (VAM) and suction casting unit.



**Figure 2.** Pictures of different cast wedges of Zr based BMGMC made from vacuum arc melting and Cu mold suction casting. (a)  $Zr_{47.5}Cu_{45.5}Al_5Co_2$  alloy without inoculants (miss run); (b)  $Zr_{47.5}Cu_{45.5}Al_5Co_2$  without inoculants (proper riser); (c)  $Zr_{47.5}Cu_{45.5}Al_5Co_2$  without inoculants (another view); (d)  $Zr_{65}Cu_{15}Al_{10}Ni_{10}$  without inoculants; (e)  $Zr_{47.5}Cu_{45.5}Al_5Co_2$  (with 0.25 wt.% inoculant 1); (f)  $Zr_{47.5}Cu_{45.5}Al_5Co_2$  (with 0.50 wt.% inoculant 1).

be seen that it is defective part with improper filling also known as miss run. This type of defect result from insufficient super heat to liquid metal which does not provide enough fluidity required for casting a sound part. It can also result from insufficient metal as a whole. That is, not enough metal was available to feed the casting geometry and provide any riser to compensate for shrinkage on top. Thus a misrun occurred. This casting is also accompanied by very rough/poor surface finish which accounts for improper use of mold coatings or too cold mold surface which causes a surface (skin) chill while rest of metal still remains to be filled. They severely affect part performance and mainly are major reasons of rejections. **Figure 2(b)** shows another wedge casting of same  $Zr_{47.5}Cu_{45.5}Al_8Co_2$  alloy made in water cooled Cu mold. This is much better casting. Defects present previously are almost eliminated and a good surface finish is obtained as well. No mold coatings are used indicating that only proper control of metal temperature (super heat) and providing enough material at top can result in production of good quality sound casting. **Figure 2(c)** is another view of same casting indicating its high quality and good dimensional accuracy. A button shape piece placed alongside wedge is riser which is cut from top portion of wedge. It is made from purposefully supplied excess material to account for any shrinkage and feed the wedge shape casting beneath. Shine of cut surface is also indicative that a good quality casting is produced free from casting defects such as porosity, pinholes and gas holes. It is also a measure of good vacuum and processing conditions in chamber. Shine at the tip region of wedge is also qualitative visual indicative of formation of glassy structure (which will be verified later by DSC). A small metal piece is cut from tip to make specimen for differential scanning calorimetry (DSC) and inductively coupled plasma (ICP) analysis. Cut made was neat and clean without any burr, chip or edge loss which again is indication of good casting quality. **Figure 2(d)** is picture of second hypoeutectic alloy  $Zr_{65}Cu_{15}Al_{10}Ni_{10}$  casted without inoculants. Again, good quality of casting can be seen and is attributed to good processing conditions, their careful control and good casting design (*i.e.* enough liquid metal at top to feed casting beneath to counter casting shrinkage). A small dimple on the riser is formed as a result of shrinkage and is indicative of good fluidity of this alloy as compared to previous one. This also helps in feeding shrinkage defect and removal of casting inhomogeneities. This wedge is shinier than previous eutectic alloy which again is due to the fact that good control of casting conditions result in the formation of sound casting and inherent fluidity of alloy contributes well to this. A small portion is removed again from tip region for microstructural and DSC analysis. This tip is mounted in epoxy resin with cut surface down to observe features evolved during solidification of casting. Finally, **Figure 2(e)** and **Figure 2(f)** are of wedges casted with 0.25 wt.% and 0.5 wt.% inoculant 1 in eutectic  $Zr_{47.5}Cu_{45.5}Al_8Co_2$  system. As can be seen and was expected, the quality of casting deteriorated with the addition of inoculants. While the effect of inoculants in changing the num-

ber density, size and distribution of ductile phase will become evident in later study aimed at microstructural investigation. Overall macro structural features of casting are severely hampered by inoculation treatment. Casting fluidity severely decreases which result in development of surface roughness and this roughness increase as percentage of inoculants increase (**Figure 2(e)** and **Figure 2(f)**). The effect becomes severely evident at higher percentage and even miss run occurred in casting with 0.5 wt. % inoculants. This is attributed to inherent ability of inoculants to increase the sluggishness of already sluggish eutectic system by acting as medium to disrupt the forces by which atoms or molecules interact in liquid melt of alloy. In worst case scenario, they may remain suspended as foreign objects in melt contributing towards overall increase of resistance to flow. This effect must be avoided at all costs to get good quality castings [73]. Although, edge to edge matching (E2EM) [74] [75] study was conducted to select potent nuclei, this is based on solid state crystallography and does not take into account the transport phenomena involved in liquid state processing which is the main reason for increase of viscosity. Even increase in super heat to cater for this decrease in fluidity does not appreciably change the flow behavior of alloy. Shrinkage at top of riser also disappear indicating decrease in fluidity [76]. Foreign particles may have created an effect in which alloy tend to stick to wall of container rather than flow alongside it. Surface tension of alloy also appears to have been affected by this anomaly. However, brittleness of alloy at tip appears to decrease a lot as a result of this treatment. This was observed while cutting small portions from tip region of “as cast” wedge samples with inoculants. Though rough in shape, it became easy to cut the alloy as the percentage of inoculants increase. This is positive and encouraging result and is indicative of the effectiveness of inoculation treatment. However, its further investigation and validation by proper metallographic and microscopic studies is pending. In general, suppressed kinetics and deep undercooling is observed at tip region while appreciable kinetics is responsible for phase formation and evolution in wider portion of wedge. This trend is appreciably affected by inoculation treatment which will be described in detail in later section (Section 3.2).

### 3.2. Microstructural Explanation

As reported previously [72], three types of grain are observed in thin section castings resembling tip region of wedge shape castings. These are namely a) mold surface grains, b) equiaxed grains and c) intermediate grains. They are explained in more detail as follows; *First category* consists of grains that form at or very near to mold wall. They are the product of very rapid rate of heat transfer [77] [78] [79] at mold wall surface thus their growth is suppressed resulting small grain having only one primary dendrite. Typically, only trunk is observed in very thin sections having thickness < 10 mm. *Second* set of grains are formed as a result of heterogeneous nucleation in the bulk of liquid. They experience relatively slow rate of cooling as compared to previous category and since they

are formed in the bulk, they are mostly equiaxed. They consist of small to medium size grains spread evenly in the matrix. Most of their growth occurs under steady state heat transfer conditions where heat consumed (endothermic reaction) from phase transformation is compensated by heat supplied from pouring hot liquid metal. The *third category* is a set off grains which are formed “between first category and equiaxed” or “between first category and center of casting”. They predominantly have two types of morphologies; namely smaller than equiaxed or more elongated than equiaxed (along one axis). Schematically they are shown in **Figures 3(a)-(c)**.

They are formed as a result of somewhat intermediate transient heat transfer conditions. These conditions are based on fluctuating rate of heat transfer in different section of the castings thus their morphology and shape also varies. A typical grain structure profile across wedge is shown in **Figure 4(a)** obtained with digital microscope with Z stacking after mild HF etching. The region identified on the basis of grain structure and morphology observed are schematically described in **Figure 4(b)**.

### 3.3. Chemical Analysis (Inductively Coupled Plasma (ICP) Analysis)

For the purpose of verifying casting quality and counter checking charge calculations, chemical composition of final cast wedge was carried out with inductively coupled plasma—optical emission spectroscopy (ICP-OES) analysis. Samples were prepared by accurately weighing and digesting 0.1 gram of alloy in a mixture of 1ml 48% HF, 2 ml 69% HNO<sub>3</sub> and 3ml of high purity (Milli-Q) water in Teflon beakers with gentle warming on a hot plate. Once the reaction has ceased, 8 ml of 4% Boric acid solution was added to complex any residual HF. Once the solutions had cooled to room temperature, they were made up to 10 ml in volumetric flasks with Milli-Q water and analyzed by Varian 730-ES axial ICP-OES. Certified multi element solutions were used to check the accuracy of the calibration standards used and the method adopted. Results are tabulated in below table (**Table 1**) for different samples.

It is quite clear that resultant compositions after analysis are very near to

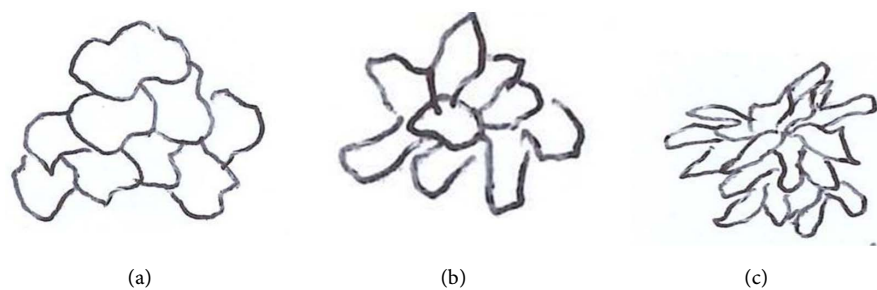


**Figure 3.** Different morphologies of grains formed during solidification in wedge castings (a) equiaxed grains (form in the bulk as a result of heterogeneous nucleation); (b) smaller than equiaxed; (c) elongated than equiaxed (along one axis).

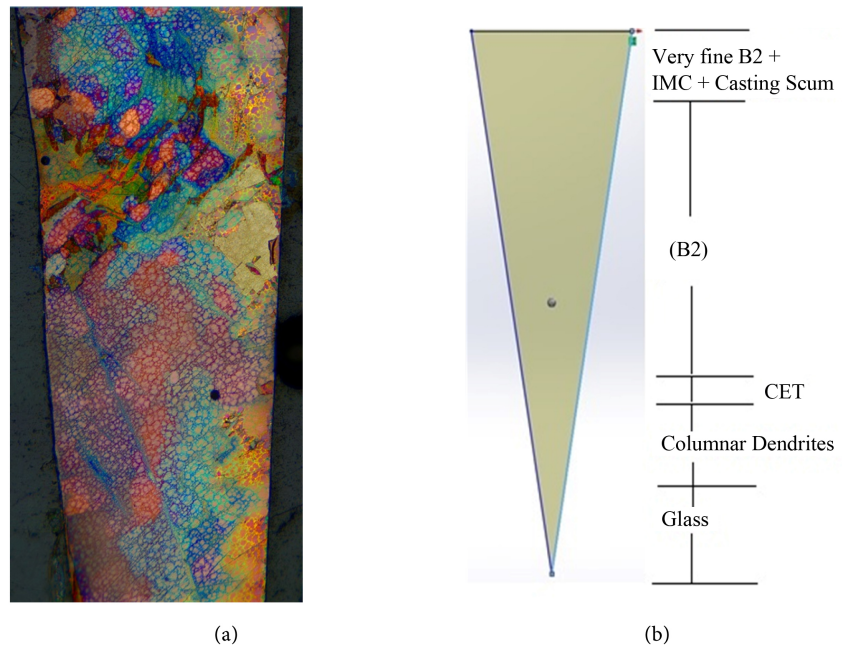


**Figure 4.** (a) Digital optical micrograph of wedge tip ( $Zr_{47.5}Cu_{45.5}Al_8Co_2$ ) after HF etching with Z stacking (obtained with Leica® digital DVM microscope); (b) Schematic of grain type distribution.

**Table 1.** ICP analysis of Zr based BMGMCs.

Sr. No.	Sample name	Al (wt.%)	Co (wt.%)	Ni (wt.%)	Cu (wt.%)	Zr (wt.%)
1	Reference (aim)	1.8	1.576	0	38.66	57.9
2	$Zr_{47.5}Cu_{45.5}Al_8Co_2$	1.79	1.76	0	41.8	55.2
3	$Zr_{47.5}Cu_{45.5}Al_8Co_2$	1.9	1.59	0	39.3	55.5
4	Reference (aim)	3.479	0	5.29	14.75	76.47
5	$Zr_{65}Cu_{15}Al_{10}Ni_{10}$	3.27	0	5.55	16.3	74.3

aimed values which indicate good process control and consistency of operation. The results in case of hypoeutectic alloys are not very well in agreement with aimed values. This happened due to slight malfunctioning of machine on test day, leak in vacuum or vaporization of high vapor pressure elements. Increase in Cu and Ni content is however due to either ICP-OES error or over calculations of charge which were done based on experience and to cater the volatility of Al and Ni but gave erroneous results. Still, these are within range of experimental error.

### 3.4. Nondestructive Testing (NDT)

Conventional nondestructive (NDT) testing techniques such as radiography and dye penetrant testing (DPT) are performed on wedge shape castings to determine surface, subsurface and internal defects, structural and chemical in-homogeneities and surface features. These are explained in detail below.

### 3.4.1. Radiography

Radiography is one of the oldest and well established techniques to determine surface, subsurface and internal defects. Its use is very well documented and is a very good estimate of casting quality and homogeneity. In general radiography is very well suited to determine hairline cracks, center line cracks, scabs, fissures, misrun, inclusions, segregation and hot tears. They image the defective area on a photographic plate as a result of exposure of sample to X-rays. The areas high in density (well casted dense metal) absorb more X rays and transmit less thus appear white and vice versa. This feature can be effectively used to identify a range of casting defects [73] [76]. ASTM Method E1742/E1742M-12 is used for carrying out radiography on wedge shape castings. Rigaku 140 KV X-ray source was used for 5 and 50 seconds. The standoff distance (*i.e.* source to film distance) is kept at 750 mm. ASTM Image Quality Indicator (IQI) IA6 are used and Pb screen was used as imaging film. Individual casting was separately exposed and different features were observed. These are explained in detail below.

These pictures clearly show different types of defects in individual wedges. Castings of  $Zr_{47.5}Cu_{45.5}Al_8Co_2$  (**Figure 5(a)** and **Figure 5(b)**) have clear demarcations. **Figure 5(a)** indicates dense and less dense inclusions by virtue of less and dense regions in the casting which arise from bad melting practice, improper

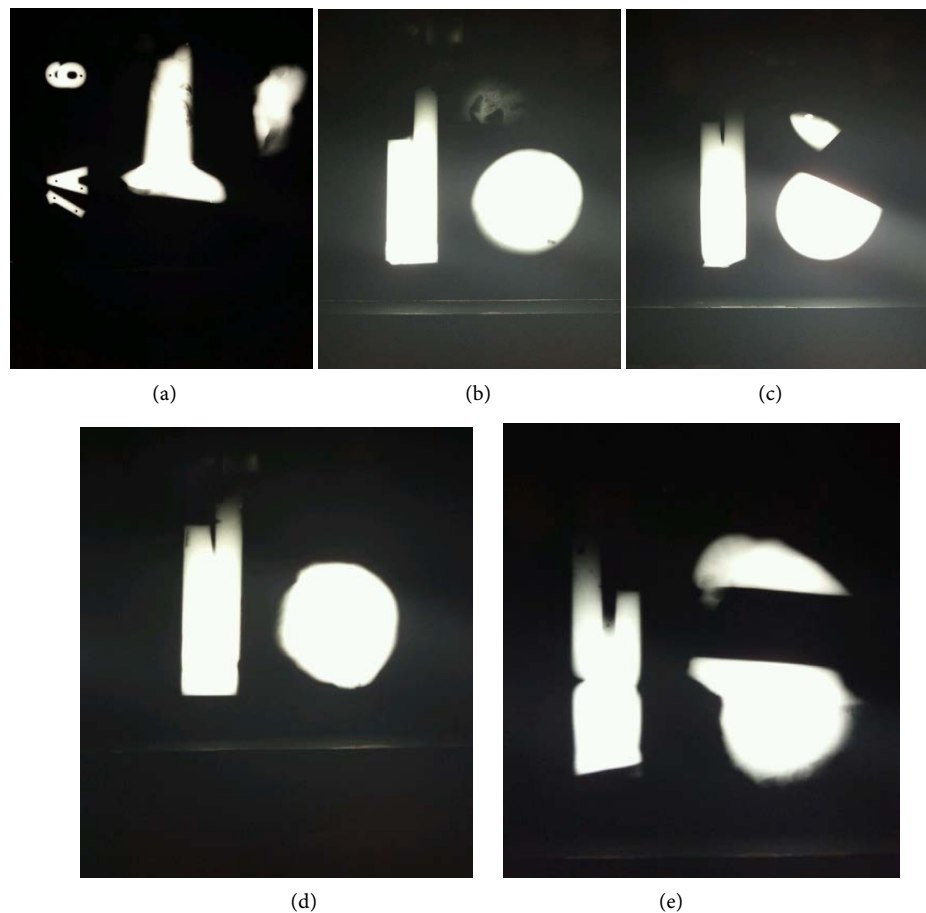


**Figure 5.** (a)-(e) Radiography examination of “as cast” Zr based BMGMCs.

vacuum in the chamber, poor control of experiment, improper homogeneity, oxidation and improper control of melt temperature or improper control of suction pressure. All or any of these parameters create a chemical and/or physical barrier which cause the formation of unwanted/unmelted particles in the system and they float to top/disperse into different regions (segregation) of castings which cause appreciable decrease in fracture toughness of material. However, it is hopeful and good news that these inclusions form only at or near top of casting. This is indication of good control of casting process as complete melting occurred and it forced the foreign/unmelted particles to gather only in regions which later can be easily removed by machining. **Figure 5(b)** also indicates dense inclusions and possible air lock caused by entrapment of air during casting (suction). This air may have formed as a result of quick incipient reaction between constituents of alloy, reaction between alloy and any dirt/grease on mold wall or by small leak in vacuum which may become visible during suction and sucks the air into permanent mold cavity and where it gets stuck in liquid metal and become part of it. Care should be taken to avoid this. Possible means of doing these include; 1) proper cleaning and degreasing of mold surface prior to inserting in the chamber 2) use of mold coatings (scavengers) which preferentially react with oxygen to form compounds (oxides) which may float on the riser during solidification and later can be removed and/or 3) mold heating to a temperature slightly above boiling point of water and preferably above boiling point of known organics in foundry. This ensures removal of water, unwanted dirt, grease, volatiles in the form of gas which can be sucked out of vacuum chamber prior pouring. This usually is not the very easy method to adopt from practical point of view because it is very difficult to insert heating mechanism in such small wedge shape mold but still is most effective and widely used approach in large molds [77]. **Figure 5(c)** is the best of casting produced and examined. It is  $Zr_{65}Cu_{15}Al_{10}Ni_{10}$  alloy which is known to have better fluidity than its eutectic counterpart. Thus, it forms the best wedge observed and examined by radiography so far. Nearly no defect is observed and as will be observed in dye penetrant testing (next section), it is almost defect free casting. Only minor dense inclusions are seen in radiograph which is attributed again to reasons just mentioned. Most likely, they are external foreign dirt stuck to wall of mold; remain in chamber or unmelted powder from charge (raw material) which got dispersed into chamber and mold cavity during arcing and then float to top during casting. **Figure 5(d)** is  $Zr_{47.5}Cu_{45.5}Al_8Co_2$  with 0.25 wt.% of inoculant A. As expected, after the addition of external particles (inoculants) the casting properties of alloy are severely affected. It became more sluggish and hard to flow which severely hampers its castability. Cracks, gas porosity and shrinkage are observed in radiograph. These are typical defects which are formed once an alloy loses its fluidity. One of possible reasons of cracking is misrun. That is alloy was never able to attain enough velocity and fluidity to cause 100% mold fill. Its gets solidified in the form of thin skin along the wall of mold very quickly before its two fronts

(one coming from top to bottom and other from bottom to top) can meet. A misrun is extremely bad and usually reported as 100% rejection. Strategies to avoid this again are mold heating or suppressants of viscosity which retard the formation of thick constituents and promote increase of fluidity. Cracks are possible off shoot of misrun. These primarily form as result of difference of temperature in different parts of casting. That is a region of casting get solidifies very quickly as compared to other and a stress is created which when reaches yield strength of material and crosses it, results in cracking. This again should be avoided by proper mold design, section thickness of casting, and avoidance of sharp corners, bulges and turns. In our case, these were inevitable as the section thickness was deliberately changed thus generation of stresses is eminent. Only their effect can be minimized by proper control of casting process and or alloy handling. Shrinkage is another big problem in castings. Like others, it also occurred in our wedges and result in small dimple on top of mold. However, its effect was not that harmful as its effect was taken care of from lesson learned by first casting. That is, a proper well designed riser and ingate combination was introduced on top of casting. Thus, even if there occurs a shrinkage, there is always enough metal available at the top which could feed volume decrease below. Its effect is more detrimental in large castings where proper gating and riser design procedures should be adopted and applied [76]. These defects become more prominent and visible as the weight percentage of inoculant particles is increased (**Figure 5(e)** (05 wt.% inoculants)). This is interesting phenomena as it is not known whether there exists a threshold till which an inoculant be added to get superior properties and beyond which properties will decrease. More research is need in his area and proper statics method should be applied to predict material properties and performance (It is part of present project and its outcomes will be described in a later study).

#### **3.4.2. Dye Penetrant Test (DPT)**

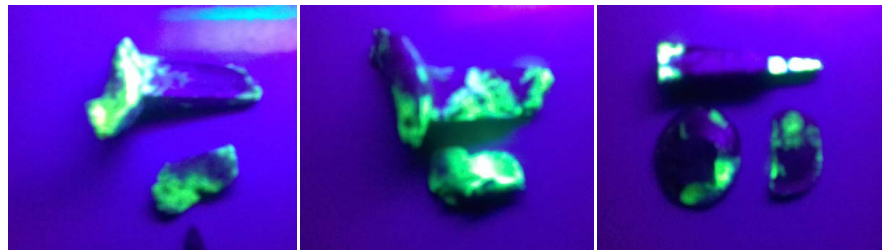
Dye penetrant testing/Liquid penetrant testing is another nondestructive method which was selected for alloy castings because of its ease of usage, well established procedures and standards, reproducibility, remoteness, quick, recyclability and physical nature. In addition to this, it can be safely applied to nonferrous metals and alloys which is part of my studies. It is not harmful to human and no serious hazard is associated with its application. It is also very robust and detailed for surface and intricate defects. ASTM E 1417 was adopted as reference and qualification standard. Procedure involve spreading a fluorescent dye on the clean (dirt and grease free) surface of metal piece followed by part observation under a UV light.

Fluorescent material applied to surface of casting are very sensitive to Ultra-violet (UV) light as the casting wedge is exposed to UV light in dark room a glowing pattern indicating the presence of surface discontinuities appear. The sharpness of this pattern depend on 1) fluorescent material used 2) nature, type, size and age of UV lamp/torch, 3) exposure time after application of dye 4) time

between application of dye and exposure and 5) amount of florescent material applied. This is well defined in ASTM E 1417 and care must be taken to adopt it and operator/inspector must adhere to it. **Figure 6(c)** and **Figure 6(g)** are  $Zr_{47.5}Cu_{45.5}Al_8Co_2$  alloy without inoculants. Typically, it can be seen that a lot of defects exist in the casting. These include surface cavity, poor feed, misrun and premature cooling (skin solidification). The pattern however, changes significantly in second experiment. As observable, sample is much more homogeneous and dense. Surface discontinuities and major defects are no more observed. Only slight linear discontinuities are observed at tip and wider part of wedge where it is cut from riser. It is envisaged that these linear discontinuities are not casting defects but effect of thermal stresses remnant in material as it is cut from these places for making sample for DSC and removal of riser head. This fact is verified by position of their occurrence and prior treatment history which is very evident to confirm their occurrence. Defects are further removed at all and completely disappear in third casting which consists of  $Zr_{65}Cu_{15}Al_{10}Co_{10}$  without inoculants. As expected, observed earlier in radiography and discussed, its reasons are pretty much the same that material is very fluid and nicely fills the mold cavity without creating unnecessary surface discontinuities and defects. Surface cavity however is observed in fourth casting which is formed after addition of 0.25 wt.% of inoculant 1 in melt. The effect of inoculation on microstructure and grain formation will be discussed later but for the time being it is very clear that a lot of surface discontinuities including roughness, improper fill and skin crust formation are very evident when external particles are added to  $Zr_{47.5}Cu_{45.5}Al_8Co_2$ . This is a direct consequence of decrease in metal velocity and increase in its viscosity. The fact become more prominent and even center line crack is observed when percentage of inoculants are increased to 0.5 wt.%. It is not known what is the effect of this increase on shape of casting? As no data exists from experiments on these alloys in industry. This is the first study of its kind aimed at studying the velocity, viscosity, fluidity and mechanical properties of these alloys as a function of its constituents.

### 3.5. Thermal Analysis (Differential Scanning Calorimetry (DSC))

Thermal analysis in the form of differential scanning calorimetry (DSC) was performed on casted BMGMC samples (namely  $Zr_{47.5}Cu_{45.5}Al_8Co_2$  and  $Zr_{65}Cu_{15}Al_{10}Ni_{10}$  respectively) without inoculants only. The aim was to ascertain if any glass structure is formed by studying glass transition temperature ( $T_g$ ) as well as structural relaxation (devitrification) ( $T_x$ ) temperatures which help to identify the temperature at which glass transforms to crystalline products. Small samples which were cut from tip of BMGMC wedge were heated in Netzsch STA 449 F1 system fitted with steel furnace and p-type DSC sensor. Alumina ( $Al_2O_3$ ) pan was used and was heated to 650°C at a rate of 20°C/min in Argon atmosphere in accordance with previously reported values [80]-[85]. An optimized higher heating rate of 20°C/min was chosen as lower rates are observed [86] to



(a)

(b)

(c)



(d)

(e)

(f)



(g)

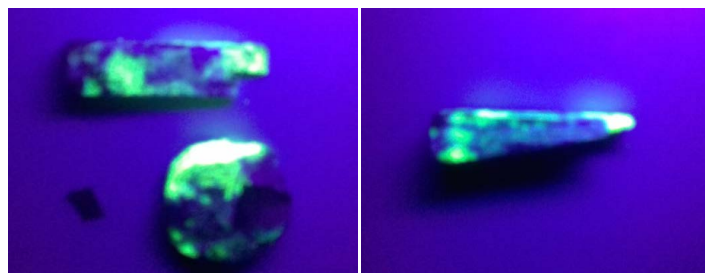
(h)

(i)



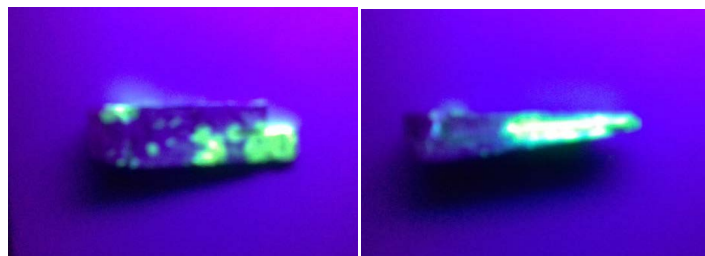
(j)

(k)



(l)

(m)



(n)

(o)

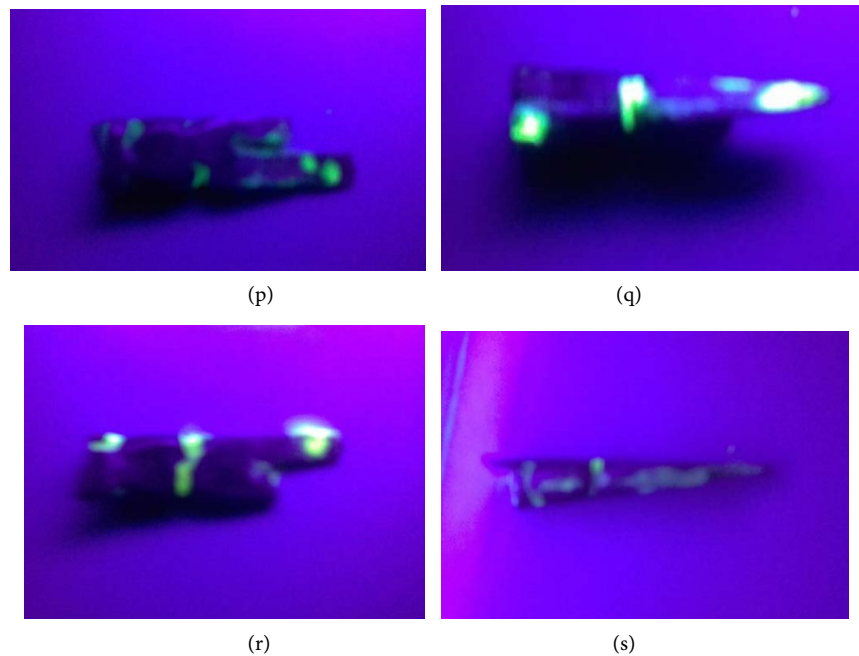


**Figure 6.** (a)-(s) UV light fluorescent pattern of cast wedges after application of dye and exposure; (a) and (b)  $\text{Zr}_{47.5}\text{Cu}_{45.5}\text{Al}_8\text{Co}_2$  without inoculants; (c)-(g)  $\text{Zr}_{47.5}\text{Cu}_{45.5}\text{Al}_8\text{Co}_2$  without inoculants; (h)-(k)  $\text{Zr}_{65}\text{Cu}_{15}\text{Al}_{10}\text{Ni}_{10}$  without inoculants; (l)-(o)  $\text{Zr}_{47.5}\text{Cu}_{45.5}\text{Al}_8\text{Co}_2$  with 0.25% inoculant 1, (p)-(s)  $\text{Zr}_{47.5}\text{Cu}_{45.5}\text{Al}_8\text{Co}_2$  with 0.5 wt.% inoculant 1.

bypass very narrow window of glass transition ( $T_g$ ) and relaxation temperatures ( $T_x$ ) (*i.e.* material spend too much time in crystallization region such that sufficient time is allowed for proper arrangement of atoms and crystallization/relaxation itself is not observed at all). An initial blank run was run prior to carrying out actual test to set base line parameters. Over lay graph obtained is shown in **Figure 7**.

The curves clearly show different temperatures at which transitions occur. Summary of main transitions events observed in these curves are given in **Table 2**.

DSC curves are characterized by three parameters namely; peak height, peak position and peak width (area under the curve) [87]. All curves display an endothermic event, which is characteristic of glass transition temperature ( $T_g$ ) followed by exothermic event corresponding to release of heat due to crystallization. These are depicted by onset points in above figure. It was previously observed and reported [87] [88] that in the absence of any reinforcing constituent (e.g. dendrites) peak tend to occur at lower temperature and as the percentage of external constituent increase, peak shifts towards higher temperature. When present graphs are compared to previously reported data, same phenomenon was observed. This is attributed to the fact that in the absence of any reinforcements, it is easy for 100% glass to transform quickly exhibiting crystallization and as the percentage of external impulses increase, they also start contributing towards overall crystallization by their inherent intrinsic effect. Their physical

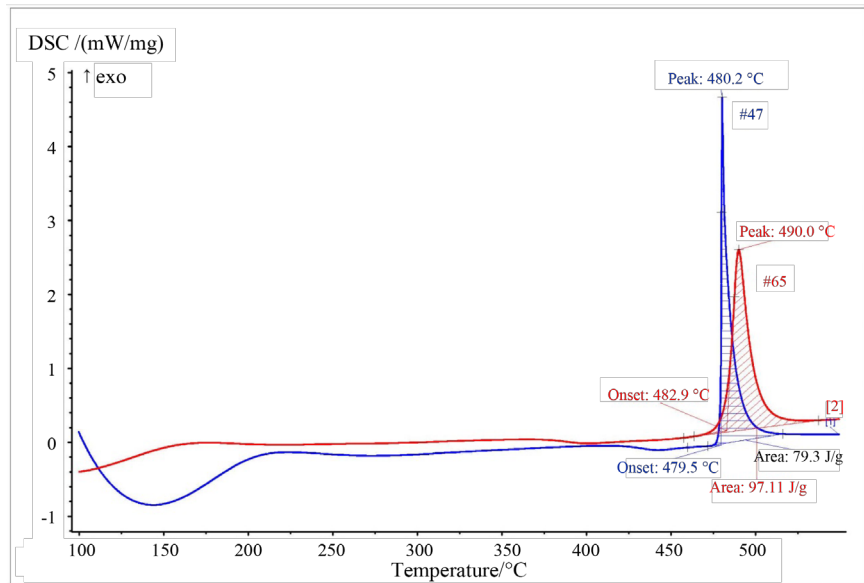


**Figure 7.** DSC curves of  $Zr_{47.5}Cu_{45.5}Al_8Co_2$  and  $Zr_{65}Cu_{15}Al_{10}Ni_{10}$  alloys.

**Table 2.** Major invariant temperatures tabulated for both hypoeutectic and hypoeutectic alloys.

Sr. No.	Alloy	$T_g$ (°C)	$T_x$ (°C)	Peak Temp (°C)	Area (J/g)
1	$Zr_{47.5}Cu_{45.5}Al_8Co_2$	423	479	480.2	79.3
2	$Zr_{65}Cu_{15}Al_{10}Ni_{10}$	378	482.9	490	97.11

state (*i.e.* glass whiskers, vitrified/devitrified ceramic particles, nano spheres or any other morphology) starts exerting its own contribution and tends to retard crystallization of glassy matrix in BMGMC. Also peak becomes broader as the amount of ductile phase increases, indicating the range on which this transition occurs. This may be attributed to the fact that glass from region in between dendrites (interdendritic space) takes time to devitrify thus prolongs the overall time for completion of transformation (crystallization). Height of peaks are also lowered indicating that not enough glass is present to cause a sharp, high and bright peak which is hopeful and proof of fact that *in-situ* dendrite reinforced composites are formed. Area under the curve can be fitted with Johnson-Mehl-Avrami (JMA) equation and used to calculate crystallized fraction at certain temperature as function of time. This may be described as follows

$$\ln\left(\frac{\alpha}{T_p^2}\right) = \ln C - \frac{E}{RT_p} \tag{1}$$

where

$E$  = Activation energy,  $\alpha$  = speed of heating,  $T_p$  = Temperature of peak and  $C$  = Crystallized fraction

For a specific temperature  $C$  can be calculated as a function of time and gives a measure of time necessary to anneal a sample at a given temperature to control the crystallized fraction.

### 3.6. Castability/Mold Fill Analysis/Characteristics

Mold fill characteristics of BMGMC are also unique. Typically, they are sluggish alloys which do not have very good casting properties such as fluidity, mold fill ability and high temperature thermal and chemical stability. Conventional casting methods such as sand casting, investment casting or even permanent mold casting have not been able to induce enough heat extraction effect, capability and capacity to reach cooling rate of the order of  $10^4$  K/sec necessary to achieve glassy structure in these alloys. It is necessary to involve suction effect (unique technique) along with water cooling in the exterior of permanent Cu mold to achieve extremely high cooling rates to manufacture these alloys. Largely, the percentage by which mold is filled during a run remains a function of transformer frequency, arc temperature, arc maneuverability (skill of operator), super heat given and rate by which Ar is removed from chamber by vacuum pump. Out of these, arc maneuverability is how skillfully arc is controlled on melt piece in button furnace. It largely determines the heat transfer pattern to and from specimen. There may be other factors also such as mold size, its geometry, riser size, runner type, suction pressure, rate by which it is applied that are responsible for mold filling but largely it remains as function of main machine parameters which are transformer frequency and rate of removal of Ar from chamber as a result of application of vacuum (suction). Other stray at maintaining their unimportant position.

### 3.7. Optical Microscopy

Casted samples were cut from the tip region in two halves and mounted in epoxy molds with fresh cut surface down to expose the surface for microstructure analysis as shown in **Figure 8** below. The samples were ground with series of emery paper with increasing finer grit and finally treated with diamond paste to metallographic finish. They were subsequently treated with etching reagent consisting of 4 ml HF (35% conc.), 4 ml HNO<sub>3</sub> (67% conc.) and 192 ml demineralized water. Total etching time was 12 - 15 seconds for eutectic and just 2 second for hypoeutectic alloys as later has very high reactivity towards acid solution. Three micrographs of each sample were taken each at tip, middle and widest region of wedge shape sample. These are shown below. First set of figures (**Figures 8(a)-(c)**) shows the microstructure of eutectic cast alloy. It clearly shows glassy matrix with finely dispersed spheroidal like crystals of primary CuZr B2 phase. Their spheroidal like acicular morphology indicates they are so called “*in-situ*” formed during solidification of casting. Another reason for appearance of this morphology is extremely high cooling rate which suppress kinetics to such a level that almost zero crystallization is observed. This is in contrast to well defined spherical morphology of B2 phase observed in alloys as a result of precipitation from melt. This is typical microstructure which is supportive of nucleation and growth phenomena. “*In-situ*” feature, on the other hand is attributed to product of a chemical reaction (reversible or irreversible) (e.g. B2 - B19) [89] which may

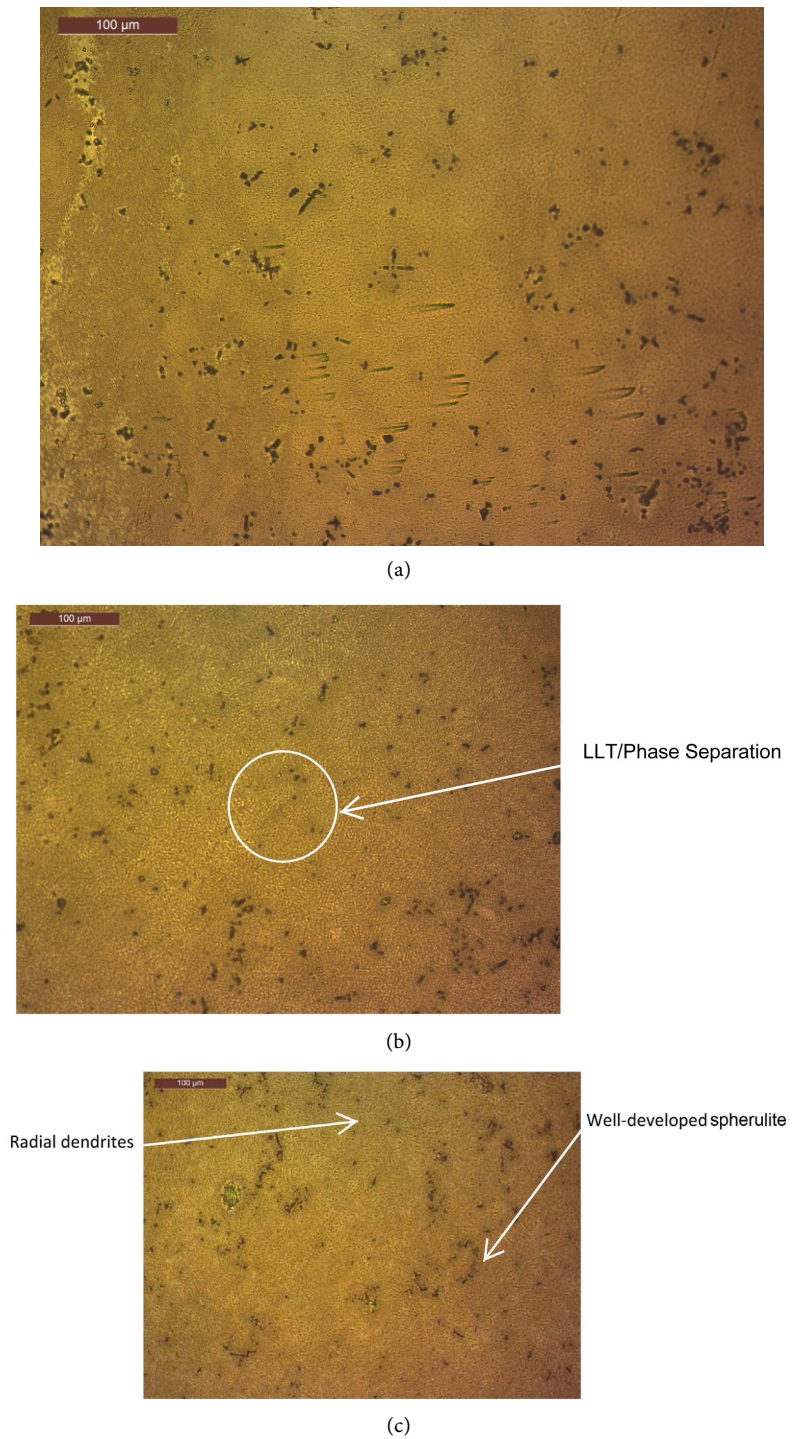
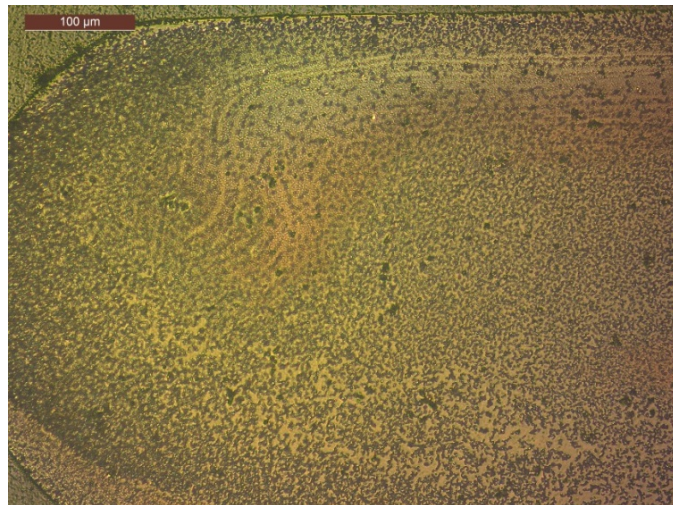


**Figure 8.** Reflected light optical micrograph  $Zr_{47.5}Cu_{45.5}Al_5Co_2$  etched ( $HF + HNO_3 + H_2O$ ) (a) tip region (200 $\times$ ); (b) middle of wedge (200 $\times$ ); (c) wider portion of wedge (200 $\times$ ).

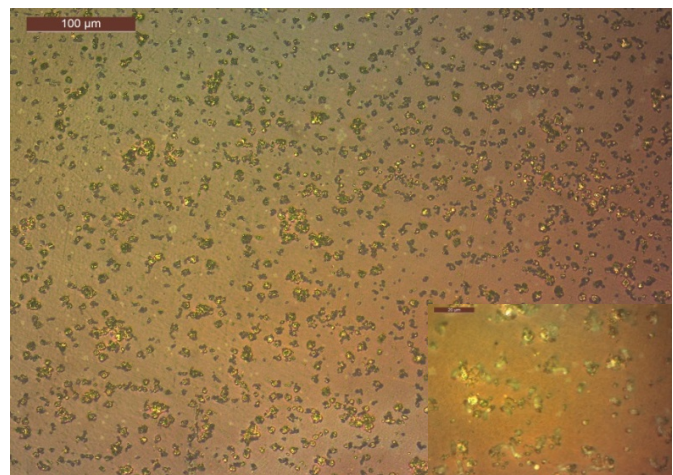
give rise to fine spheroidal like or spherulitic microstructure with very sharp edges. The volume fraction ( $V_f$ ) of these spheroidal like crystals increase with the change of cooling rate as we travel towards wider portion of wedge. Higher percentage of glass is present at the tip indicating maximum cooling rate and sup-

pression of kinetics. As the distance from tip increase, appearance of other features starts appearing in microstructures. These include; slight “spotty contrast” [90] between glassy and crystalline regions. Two main reasons are corroborated for this. One is the occurrence of varying stress fields around shear bands which cause martensitic transformation of  $\beta$  phase or B2 to glass as reported in earlier study by Prof. Johnston [90] and other is relatively recently observed phenomena upon investigation of these alloys in synchrotron light termed as liquid-liquid transition (LLT) [91] [92] or more popularly phase separation [93] [94] [95]. Another feature of interest is appearance of “radial dendrites”. This is more predominantly observed in **Figure 8(c)** which is taken at widest portion of wedge at farthest distance from tip. Occurrence of these is attributed to change of cooling rate which cause thermal fields in conjunction with fluid fields promoting solute rejection, its diffusion, capillary action and CFD phenomena in such a way that dendrites grow only in certain direction with respect casting geometry [96]. Lastly, “variant contrast” is observed under reflected light microscopy as the sample is traversed in the path of light. This dull to shiny contrast is due to occurrence of varying percentage of crystalline dendrites trying to nucleate out of liquid during rapid cooling at the same time their growth is suppressed due to very high rate suppressing kinetics. A sharp dull to shiny interface is developed at the glass to crystal boundary which also indicates development of composite structure [97]. A refinement in this structure and its control is crucial for the control and enhancement of mechanical properties of these alloys. A quantitative metallography of this microstructure detailing number density ( $d_c$ ), size, distribution and occurrence of ductile phases as a function of distance from tip is pending and will be described in a later study.

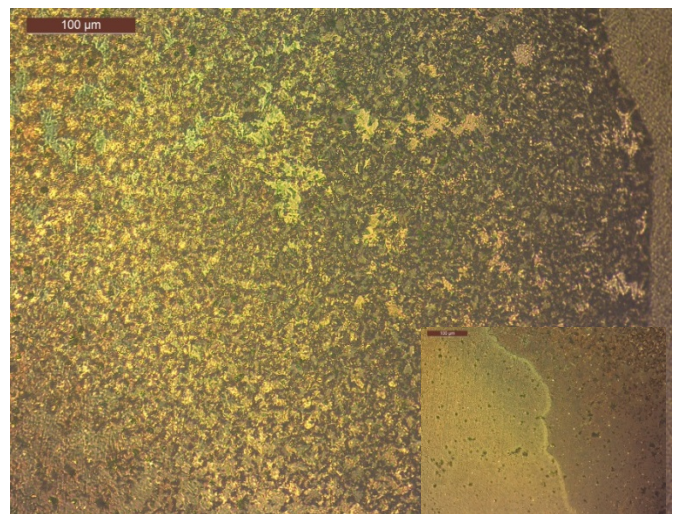
Second set of figures (**Figures 9(a)-(c)**) shows the microstructure of hypoeutectic cast alloy  $Zr_{65}Cu_{15}Al_{10}Ni_{10}$  after etching under reflected light microscopy. As described in section 3.2 above, this is the best casting obtained. Thus, matching with observations in NDT, optical micrographs show very nice microstructure of this system detailing formation, development and distribution of second phase precipitates nicely and evenly in glassy matrix. The precipitates formed are  $\beta$ -Zr whose percentage represented and measured in the form of volume fraction ( $V_f$ ) increase as the distance from tip region increases. **Figure 9(a)** depicts micrograph of alloy taken at tip region. Main features observed in this micrograph are glassy matrix represented by light color region with very fine dispersion of small nearly round precipitates all over the matrix. They are not only indicative of the development of metal matrix composite structure but also help in identifying casting features (very well defined flow lines) which are correlated with casting quantification study done in nondestructive testing. Flow patterns help identify regions of casting which experience high cooling rate and thus solidify first. This preferential solidification is the reason of macroscopic anisotropy of properties across the cross section of a casting. As the distance from tip region increases, a variation in microstructure is observed. The size of fine precipitates



(a)



(b)



(c)

**Figure 9.** Reflected light optical micrograph  $Zr_{65}Cu_{15}Al_{10}Ni_{10}$  etched ( $HF + HNO_3 + H_2O$ ) (a) tip region (200 $\times$ ); (b) middle of wedge (200 $\times$ ) inset (1000 $\times$ ); (c) wider portion of wedge (200 $\times$ ) inset (1000 $\times$ ).

gets a little bigger due to more time available for diffusion and their dispersion increases measured in the form of inter particle distance. Inset shows same microstructure at higher magnification which is representation of this well-developed morphology. A variant dull to shiny contrast also disappears because nominal composition is more fluid, does not constitute sluggishness and is the reason of retaining supercooled liquid at room temperature (glass phase). Glass is present as light areas passivated from etching reagent whereas crystalline three dimensional dendritic network is revealed as a result of its enhanced reactivity and selective leaching towards etching reagent [98]. As distance from tip increases, the percentage of glassy phase decreases and more well defined fine dispersion of ductile phase crystals nucleating from liquid increase appreciably. It appears dark because of its inability to reflect light. It promotes homogeneity which gives rise to enhanced mechanical properties. However, microstructure here is also characterized by a boundary region present in the form of an interface very near to the edge of wedge shape casting (inset of **Figure 9(c)**). This gets revealed as a result of preferential etching which gives it its characteristic light to dark contrast. It is envisaged that this occurred as a result of segregation or inhomogeneous distribution of elements because of time dependent varying (transient) casting conditions (varying cooling rate and fluctuating chemical composition) in this region under the influence of complex multiphysics phenomena. Overall crystal fraction increases appreciably in this region.

**Figures 10(a)-(c)** comprises of alloys of  $Zr_{47.5}Cu_{45.5}Al_5Co_2$  with 0.25 and 0.50 wt.% of potent inoculant. The synergic effect of inoculation is well observed and can easily be seen in the micrographs in all three areas after light etching. **Figure 10(a)** reveals the evolution of well-defined three dimensional dendritic network in glassy matrix. As a result of inoculation treatment crystalline dendrites are formed in glassy matrix. They get selectively dissolved during etching and appear as areas of dark color in light background (which is glass). Their percentage and dispersion is increased while their size gets finer as the distance from tip increases. This is again due to same reason that inoculation treatment helps improve microstructure by providing sites for heterogeneous nucleation which reduce overall undercooling required to overcome critical nucleation barrier for the formation and growth of a stable nuclei. The effect of cooling rate is that the increased percentage of fine dendrites is observed farthest from tip because of decreased cooling rate there concurrent with decrease of glass phase in that zone. Similarly, **Figures 10(d)-(f)** is another microstructure of same alloy but with increased amount of inoculant. A higher percentage (0.5%) of potent inoculant gives rise to highly developed, dense and coarse dendrites. Their dispersion increase and their number density also increase appreciably. However, a contrast in microstructure is also observed detailing light and dark areas which happens due to difference of cooling rate in two different regions of casting along the line perpendicular to major axis (**Figure 10(e)**). This is very important feature and establishes a criterion for assigning flow rate and quantification of

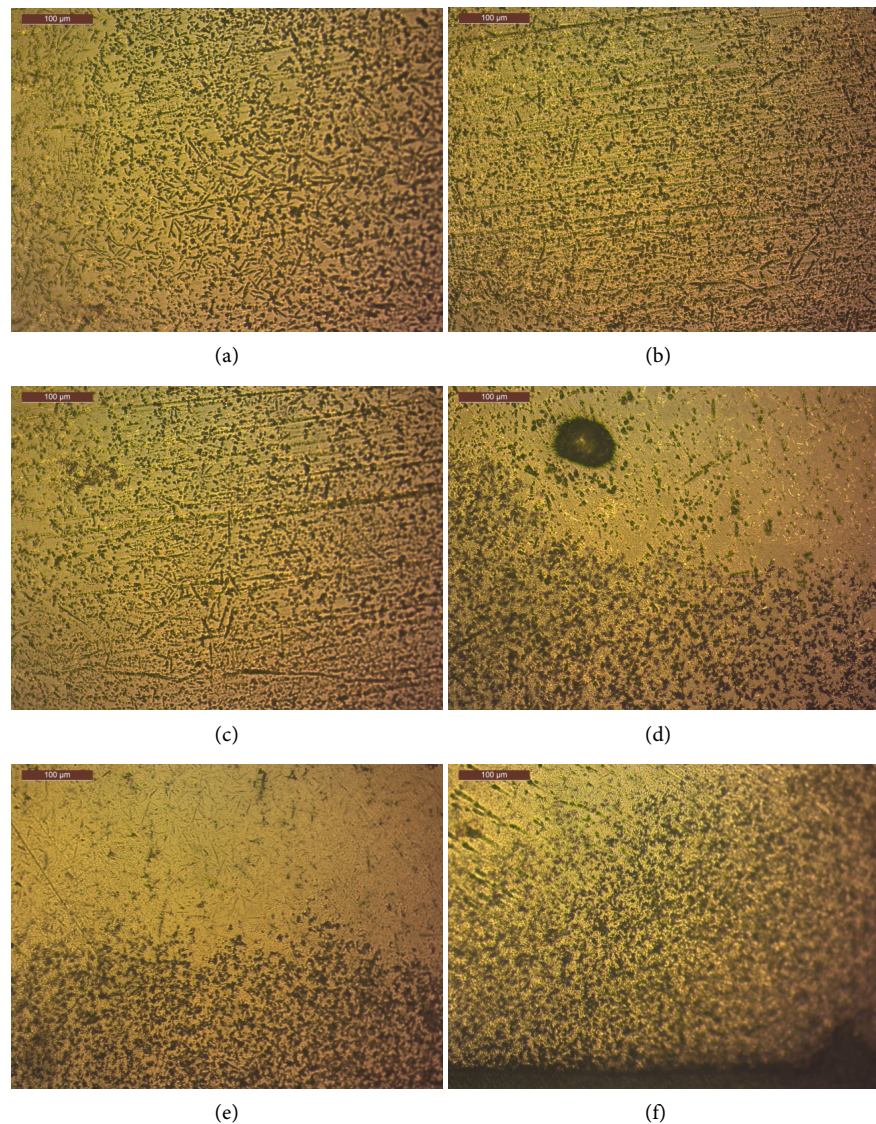


**Figure 10.** Reflected light optical micrograph  $Zr_{47.5}Cu_{45}Al_5Co_2$  etched ( $HF + HNO_3 + H_2O$ ) (a)-(c) 0.25% inoculant (a) tip region; (b) middle of wedge and (c) edge of wedge ( $200\times$ ); and (d)-(f) 0.5% inoculant (d) tip region; (e) middle of wedge and (f) edge of wedge ( $200\times$ ).

casting conditions. Typically, this is resultant of combination of cooling rate and chemical composition. Glass is observed in areas which are close to wall of casting thus having maximum possible heat extraction while ductile phase containing composite microstructure is observed as we move towards inside of casting away from wall. A very large black spot (etch pit) in **Figure 10(d)** is observed which is due to selective dissolution—a typical phenomenon observed in these alloys [98] [99] [100]. Three dimensional growth of tree like long dendrites originating from one side (wall side) of mold is characteristic of nucleation and growth driven solidification phenomena (a feature of crystalline alloys).

Overall the percentage of glass decreases while amount and dispersion of ductile dendrites increase and their size get finer as a result of inoculation treatment.

A detailed quantitative metallography of this is pending and will be described in later study.

### 3.8. Microhardness Testing

Further characterization of casting was done by carrying out Microhardness testing following ASTM E 384-16. For this purpose, a calibrated Vickers hardness tester was used with small load of 5N. The tester was calibrated first and then each specimen was tested in segments with taking three readings on each. The three readings were averaged out at the end to take final estimate of hardness. These are plotted along y-axis as a function of percentage of inoculants along x-axis in the form of graph elaborating behavior of material with inset showing schematic of wedge with positions where readings are taken (**Figure 11**).

As can be observed that hardness tends to increase from 0% - 0.25% inoculant where it is maximum and then decrease as the percentage of inoculant reaches 0.5%. This is due to the fact that increased percentage of inoculants beyond a certain limit induces strain softening effect under the tip of indenter. This may have been caused due to the fact that increased volume fraction ( $V_f$ ) of ductile phase dispersed evenly in matrix decrease the overall strengthening effect caused by glassy phase which is the main factor contributing towards hardness of these alloy systems whereas their volume fraction is not appreciable enough at 0.25% to impart overall decrease of hardness. Contrary to both, a low value of hardness at zero percent inoculant tends to suggest typical well documented strain softening effect [101] [102] under the tip of indenter and it was expected that this would have been prominent as multiple shear bands form when monolithic glass undergoes shear, free volume exists in overall matrix [103] and also rate of

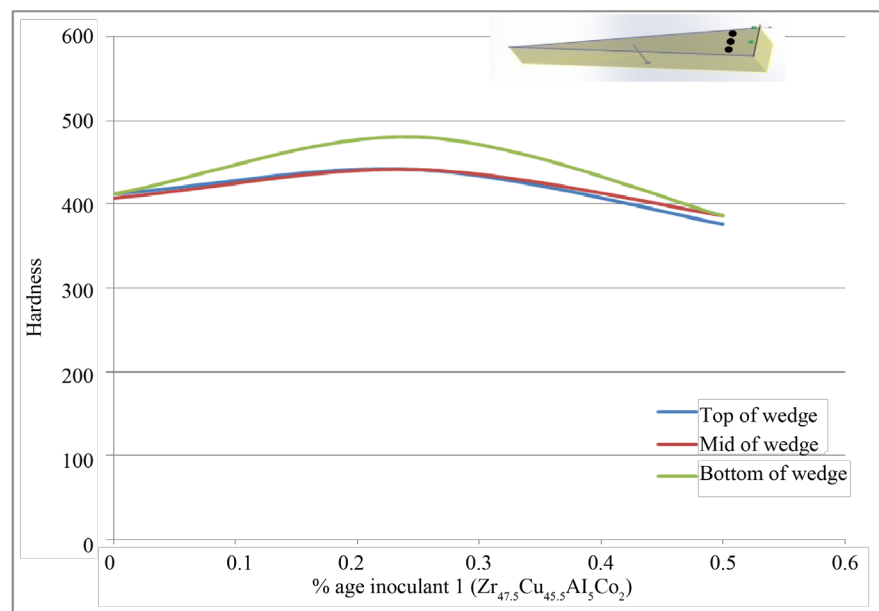


**Figure 11.** Plot of hardness vs. percentage of inoculant.

loading is uncontrolled and is very high [104] (which helps in reducing intrinsic brittleness of glassy phase—main reason of high strength). Another important feature to observe is variation of hardness at different location of point of test. It can be clearly seen that hardness is highest at a point near the bottom of wedge and it decreases as this point is moved upwards. This is in conjunction with earlier observations made in section 6 above which shows that distinct flow patterns formed as a result of variant CFD along section thickness. This gives rise to development of different percentages of volume fraction ( $V_f$ ) of ductile phase in different regions thus promoting contrast in mechanical properties.

#### 4. Conclusions

Following conclusions can be drawn from melting, casting and inoculation of bulk metallic glass matrix composites (BMGMC) in vacuum arc melting and suction casting.

1) Bulk metallic glass matrix composites (BMGMC) are very sluggish and difficult to cast alloys. Vacuum melting and suction casting is effective way to fabricate these alloys. However, extremely careful control and monitoring of process variables is needed to form these alloys in good shape.

2) Wedge shape castings of BMGMC were made to study the effect of inoculation and cooling rate on castability, phase formation and its transformation.

3) Chemical (Inductively coupled plasma (ICP)), thermal (DSC) and Nondestructive testing (Radiography and dye penetrant testing (DPT)) are performed to ascertain composition, crystallization behavior, quality, homogeneity and integrity of casting.

4) Hypoeutectic systems are found to possess good casting properties (fluidity, mold filling, and thermal stability) as compared to eutectic compositions for a fix shape of wedge casting.

5) Thermal analysis can be tentatively correlated to percentage of glass and percentage of crystal phase in BMGMCs. Crystallinity is attributed to formation of ductile phase during solidification.

6) Optical microscopy and micro hardness testing further verify and counter check the results and facts observed in previous treatment indicating effectiveness of inoculation treatment.

Overall, this study provided a first footprint of manufacturing of these alloys by controlled inoculation which will lead to denser and tougher alloys belonging to this family to serve the purpose of competent engineering material of future.

#### Acknowledgements

Authors would like to acknowledge Dr. Dong Qiu for guidance, support and motivation throughout this work and to Prof. Mark Easton for positive criticism and helpful discussion. Author would also specially like to thank Dr. Daniel East (CSIRO) for support all throughout stay at CSIRO including use of Vacuum Arc Melting (VAM) and suction casting button furnace and helpful discussion. Dr.

Yeşim M. Gözükarar (CSIRO) for conducting detailed DSC analysis. Dr. Winston Liew (CSIRO) for conducting detailed ICP analysis and Staff and personal at Aben Technical Services Pty Ltd. Victoria for conducting Nondestructive tests and providing technical and background support.

### Competing Financial Interests

The author(s) declare no competing financial interests.

### References

- [1] Hofmann, D.C., *et al.* (2015) Hypervelocity Impact Testing of a Metallic Glass-Stuffed Whipple Shield. *Advanced Engineering Materials*, **17**, 1313-1322. <https://doi.org/10.1002/adem.201400518>
- [2] Davidson, M., *et al.* (2013) Investigating Amorphous Metal Composite Architectures as Spacecraft Shielding. *Advanced Engineering Materials*, **15**, 27-33. <https://doi.org/10.1002/adem.201200313>
- [3] Jiang, J.-Z., *et al.* (2015) Low-Density High-Strength Bulk Metallic Glasses and Their Composites: A Review. *Advanced Engineering Materials*, **17**, 761-780. <https://doi.org/10.1002/adem.201400252>
- [4] Tong, X., *et al.* (2016) Structural Evolution and Strength Change of a Metallic Glass at Different Temperatures. *Scientific Reports*, **6**, Article No. 30876. <https://doi.org/10.1038/srep30876>
- [5] Hofmann, D.C. and Roberts, S.N. (2015) Microgravity Metal Processing: from Undercooled Liquids to Bulk Metallic Glasses. *NPJ Microgravity*, **1**, 15003. <https://doi.org/10.1038/npjmgrav.2015.3>
- [6] Kruzic, J.J. (2016) Bulk Metallic Glasses as Structural Materials: A Review. *Advanced Engineering Materials*, **18**, 1308-1331. <https://doi.org/10.1002/adem.201600066>
- [7] Hamill, L., *et al.* (2014) Hypervelocity Impact Phenomenon in Bulk Metallic Glasses and Composites. *Advanced Engineering Materials*, **16**, 85-93. <https://doi.org/10.1002/adem.201300252>
- [8] Archard, J.F. (1953) Contact and Rubbing of Flat Surfaces. *Journal of Applied Physics*, **24**, 981-988. <https://doi.org/10.1063/1.1721448>
- [9] Yang, H., *et al.* (2014) Dry Sliding Tribological Properties of a Dendrite-Reinforced Zr-Based Bulk Metallic Glass Matrix Composite. *Journal of Materials Science and Technology*, **30**, 576-583. <https://doi.org/10.1016/j.jmst.2014.05.004>
- [10] Wu, H., *et al.* (2013) Tribological Studies of a Zr-Based Bulk Metallic Glass. *Intermetallics*, **35**, 25-32. <https://doi.org/10.1016/j.intermet.2012.11.010>
- [11] Wu, H., *et al.* (2012) Dry Sliding Tribological Behavior of Zr-Based Bulk Metallic Glass. *Transactions of Nonferrous Metals Society of China (English Edition)*, **22**, 585-589. [https://doi.org/10.1016/S1003-6326\(11\)61217-X](https://doi.org/10.1016/S1003-6326(11)61217-X)
- [12] Hofmann, D.C., *et al.* (2017) Optimizing Bulk Metallic Glasses for Robust, Highly Wear-Resistant Gears. *Advanced Engineering Materials*, **19**, 1600541-n/a.
- [13] Ishida, M., *et al.* (2007) Wear Resistivity of Super-Precision Microgear Made of Ni-Based Metallic Glass. *Materials Science and Engineering A*, **448-451**, 149-154. <https://doi.org/10.1016/j.msea.2006.02.300>
- [14] Zhao, S., *et al.* (2016) Centimeter-Sized Quaternary Ti-Based Bulk Metallic Glasses

- with High Ti Content of 50 at%. *Advanced Engineering Materials*, **18**, 231-235. <https://doi.org/10.1002/adem.201500165>
- [15] Gong, P., *et al.* (2013) A New Centimeter-Sized Ti-Based Quaternary Bulk Metallic Glass with Good Mechanical Properties. *Advanced Engineering Materials*, **15**, 691-696. <https://doi.org/10.1002/adem.201200391>
- [16] Komatsu, K., *et al.* (2015) Zr-Based Bulk Metallic Glass as a Cylinder Material for High Pressure Apparatuses. *High Pressure Research*, **35**, 254-262. <https://doi.org/10.1080/08957959.2015.1041939>
- [17] Yi, J., *et al.* (2014) A Damage-Tolerant Bulk Metallic Glass at Liquid-Nitrogen Temperature. *Journal of Materials Science and Technology*, **30**, 627-630. <https://doi.org/10.1016/j.jmst.2014.04.017>
- [18] Donovan, P.E. and Stobbs, W.M. (1981) The Structure of Shear Bands in Metallic Glasses. *Acta Metallurgica*, **29**, 1419-1436. [https://doi.org/10.1016/0001-6160\(81\)90177-2](https://doi.org/10.1016/0001-6160(81)90177-2)
- [19] Dai, L.H. and Bai, Y.L. (2008) Basic Mechanical Behaviors and Mechanics of Shear Banding in BMGs. *International Journal of Impact Engineering*, **35**, 704-716. <https://doi.org/10.1016/j.ijimpeng.2007.10.007>
- [20] Greer, A.L., Cheng, Y.Q. and Ma, E. (2013) Shear Bands in Metallic Glasses. *Materials Science and Engineering: R. Reports*, **74**, 71-132. <https://doi.org/10.1016/j.mser.2013.04.001>
- [21] Yi, J., *et al.* (2016) Glass-Forming Ability and Crystallization Behavior of Al<sub>86</sub>Ni<sub>9</sub>La<sub>5</sub> Metallic Glass with Si Addition. *Advanced Engineering Materials*, **18**, 972-977.
- [22] Lewandowski, J.J. and Greer, A.L. (2006) Temperature Rise at Shear Bands in Metallic Glasses. *Nature Materials*, **5**, 15-18. <https://doi.org/10.1038/nmat1536>
- [23] Roessig, K.M. and Mason, J.J. (1999) Adiabatic Shear Localization in the Dynamic Punch Test, Part I: Experimental Investigation. *International Journal of Plasticity*, **15**, 241-262. [https://doi.org/10.1016/S0749-6419\(98\)00069-2](https://doi.org/10.1016/S0749-6419(98)00069-2)
- [24] Roessig, K.M. and Mason, J.J. (1999) Adiabatic Shear Localization in the Dynamic Punch Test, Part II: Numerical Simulations. *International Journal of Plasticity*, **15**, 263-283. [https://doi.org/10.1016/S0749-6419\(98\)00070-9](https://doi.org/10.1016/S0749-6419(98)00070-9)
- [25] Spaepen, F. (2006) Metallic Glasses: Must Shear Bands Be Hot? *Nature Materials*, **5**, 7-8. <https://doi.org/10.1038/nmat1552>
- [26] Choi-Yim, H., *et al.* (1999) Synthesis and Characterization of Particulate Reinforced Zr<sub>57</sub>Nb<sub>5</sub>Al<sub>10</sub>Cu<sub>15.4</sub>Ni<sub>12.6</sub> Bulk Metallic Glass Composites. *Acta Materialia*, **47**, 2455-2462. [https://doi.org/10.1016/S1359-6454\(99\)00103-2](https://doi.org/10.1016/S1359-6454(99)00103-2)
- [27] Deng, S.T., *et al.* (2011) Metallic Glass Fiber-Reinforced Zr-Based Bulk Metallic Glass. *Scripta Materialia*, **64**, 85-88. <https://doi.org/10.1016/j.scriptamat.2010.09.014>
- [28] Hays, C.C., Kim, C.P. and Johnson, W.L. (2000) Microstructure Controlled Shear Band Pattern Formation and Enhanced Plasticity of Bulk Metallic Glasses Containing *in Situ* Formed Ductile Phase Dendrite Dispersions. *Physical Review Letters*, **84**, 2901-2904. <https://doi.org/10.1103/PhysRevLett.84.2901>
- [29] Hays, C.C., Kim, C.P. and Johnson, W.L. (2001) Improved Mechanical Behavior of Bulk Metallic Glasses Containing *in Situ* Formed Ductile Phase Dendrite Dispersions. *Materials Science and Engineering: A*, **304-306**, 650-655. [https://doi.org/10.1016/S0921-5093\(00\)01557-4](https://doi.org/10.1016/S0921-5093(00)01557-4)
- [30] Schroers, J., *et al.* (1999) Pronounced Asymmetry in the Crystallization Behavior during Constant Heating and Cooling of a Bulk Metallic Glass-Forming Liquid. *Physical Review B*, **60**, 11855-11858. <https://doi.org/10.1103/PhysRevB.60.11855>

- [31] Matthieu, M. (2016) Relaxation and Physical Aging in Network Glasses: A Review. *Reports on Progress in Physics*, **79**, Article ID: 066504. <https://doi.org/10.1088/0034-4885/79/6/066504>
- [32] Wang, S. and Zhang, Y. (2009) Shear-Band Spacing Controlled by Bridgman Solidification in Dendrite/BMG Composites. *Science in China Series G: Physics, Mechanics and Astronomy*, **52**, 1632-1636. <https://doi.org/10.1007/s11433-009-0237-4>
- [33] Wu, F.-F., *et al.* (2014) Stabilized Shear Banding of ZrCu-Based Metallic Glass Composites under Tensile Loading. *Journal of Materials Science*, **49**, 2164-2170. <https://doi.org/10.1007/s10853-013-7909-1>
- [34] Yang, Y. and Liu, C.T. (2012) Size Effect on Stability of Shear-Band Propagation in Bulk Metallic Glasses: An Overview. *Journal of Materials Science*, **47**, 55-67. <https://doi.org/10.1007/s10853-011-5915-8>
- [35] Yang, G.N., Shao, Y. and Yao, K.F. (2016) The Shear Band Controlled Deformation in Metallic Glass: A Perspective from Fracture. *Scientific Reports*, **6**, Article No. 21852. <https://doi.org/10.1038/srep21852>
- [36] Hufnagel, T.C., *et al.* (2002) Controlling Shear Band Behavior in Metallic Glasses through Microstructural Design. *Intermetallics*, **10**, 1163-1166. [https://doi.org/10.1016/S0966-9795\(02\)00157-7](https://doi.org/10.1016/S0966-9795(02)00157-7)
- [37] Zeng, F., *et al.* (2015) Dynamic Fragmentation Induced by Network-Like Shear Bands in a Zr-Based Bulk Metallic Glass. *Intermetallics*, **56**, 96-100. <https://doi.org/10.1016/j.intermet.2014.09.008>
- [38] Zhang, H., Maiti, S. and Subhash, G. (2008) Evolution of Shear Bands in Bulk Metallic Glasses under Dynamic Loading. *Journal of the Mechanics and Physics of Solids*, **56**, 2171-2187. <https://doi.org/10.1016/j.jmps.2008.01.008>
- [39] Greer, J.R. and De Hosson, J.T.M. (2011) Plasticity in Small-Sized Metallic Systems: Intrinsic versus Extrinsic Size Effect. *Progress in Materials Science*, **56**, 654-724. <https://doi.org/10.1016/j.pmatsci.2011.01.005>
- [40] Jang, D., Gross, C.T. and Greer, J.R. (2011) Effects of Size on the Strength and Deformation Mechanism in Zr-Based Metallic Glasses. *International Journal of Plasticity*, **27**, 858-867. <https://doi.org/10.1016/j.ijplas.2010.09.010>
- [41] Jeon, C., *et al.* (2015) Effects of Effective Dendrite Size on Tensile Deformation Behavior in Ti-Based Dendrite-Containing Amorphous Matrix Composites Modified from Ti-6Al-4V Alloy. *Metallurgical and Materials Transactions A: Physical Metallurgy and Materials Science*, **46**, 235-250. <https://doi.org/10.1007/s11661-014-2531-7>
- [42] Szuecs, F., Kim, C.P. and Johnson, W.L. (2001) Mechanical Properties of Zr<sub>56.2</sub>Ti<sub>13.8</sub>Nb<sub>5.0</sub>Cu<sub>6.9</sub>Ni<sub>5.6</sub>Be<sub>12.5</sub> Ductile Phase Reinforced Bulk Metallic Glass Composite. *Acta Materialia*, **49**, 1507-1513. [https://doi.org/10.1016/S1359-6454\(01\)00068-4](https://doi.org/10.1016/S1359-6454(01)00068-4)
- [43] Raghavan, R., *et al.* (2009) Toughness of As-Cast and Partially Crystallized Composites of a Bulk Metallic Glass. *Intermetallics*, **17**, 835-839. <https://doi.org/10.1016/j.intermet.2009.03.012>
- [44] Qiao, J.W., *et al.* (2013) Dendritic and Spherical Crystal Reinforced Metallic Glass Matrix Composites. *International Journal of Minerals, Metallurgy and Materials*, **20**, 386-392. <https://doi.org/10.1007/s12613-013-0740-5>
- [45] Qiao, J.W., *et al.* (2010) Development of Plastic Ti-Based Bulk-Metallic-Glass-Matrix Composites by Controlling the Microstructures. *Materials Science and Engineering A*, **527**, 7752-7756. <https://doi.org/10.1016/j.msea.2010.08.055>

- [46] Lewandowski, J.J., Shazly, M. and Nouri, A.S. (2006) Intrinsic and Extrinsic Toughening of Metallic Glasses. *Scripta Materialia*, **54**, 337-341. <https://doi.org/10.1016/j.scriptamat.2005.10.010>
- [47] Fan, C., Ott, R.T. and Hufnagel, T.C. (2002) Metallic Glass Matrix Composite with Precipitated Ductile Reinforcement. *Applied Physics Letters*, **81**, 1020-1022. <https://doi.org/10.1063/1.1498864>
- [48] Telford, M. (2004) The Case for Bulk Metallic Glass. *Materials Today*, **7**, 36-43. [https://doi.org/10.1016/S1369-7021\(04\)00124-5](https://doi.org/10.1016/S1369-7021(04)00124-5)
- [49] Scudino, S., *et al.* (2009) Mechanical Properties of Al-Based Metal Matrix Composites Reinforced with Zr-Based Glassy Particles Produced by Powder Metallurgy. *Acta Materialia*, **57**, 2029-2039. <https://doi.org/10.1016/j.actamat.2009.01.010>
- [50] Kui, H.W., Greer, A.L. and Turnbull, D. (1984) Formation of Bulk Metallic Glass by Fluxing. *Applied Physics Letters*, **45**, 615-616. <https://doi.org/10.1063/1.95330>
- [51] He, Y., Shen, T. and Schwarz, R.B. (1998) Bulk Amorphous Metallic Alloys: Synthesis by Fluxing Techniques and Properties. *Metallurgical and Materials Transactions A*, **29**, 1795-1804. <https://doi.org/10.1007/s11661-998-0002-8>
- [52] Yamamoto, T., *et al.* (2008) Soft Magnetic Fe-Based Metallic Glasses Prepared by Fluxing and Water-Quenching. *Reviews on Advanced Materials Science*, **18**, 126-130.
- [53] Schwarz, R.B. and Johnson, W.L. (1983) Formation of an Amorphous Alloy by Solid-State Reaction of the Pure Polycrystalline Metals. *Physical Review Letters*, **51**, 415-418. <https://doi.org/10.1103/PhysRevLett.51.415>
- [54] Hofmann, D.C., *et al.* (2009) Semi-Solid Induction Forging of Metallic Glass Matrix Composites. *JOM*, **61**, 11-17. <https://doi.org/10.1007/s11837-009-0172-x>
- [55] Wang, B., *et al.* (2010) Simulation of Solidification Microstructure in Twin-Roll Casting Strip. *Computational Materials Science*, **49**, S135-S139. <https://doi.org/10.1016/j.commatsci.2010.01.051>
- [56] Jassim, A.K. and Hammood, A.S. (2016) Single Roll Melt Spinning Technique Applied as a Sustainable Forming Process to Produce Very Thin Ribbons of 5052 and 5083 Al-Mg Alloys Directly from Liquid State. *Procedia CIRP*, **40**, 133-137. <https://doi.org/10.1016/j.procir.2016.01.079>
- [57] Schroers, J., Pham, Q. and Desai, A. (2007) Thermoplastic Forming of Bulk Metallic Glass—A Technology for MEMS and Microstructure Fabrication. *Journal of Microelectromechanical Systems*, **16**, 240-247. <https://doi.org/10.1109/JMEMS.0007.892889>
- [58] Duan, G., *et al.* (2007) Bulk Metallic Glass with Benchmark Thermoplastic Processability. *Advanced Materials*, **19**, 4272-4275. <https://doi.org/10.1002/adma.200700969>
- [59] Sarac, B., *et al.* (2011) Three-Dimensional Shell Fabrication using Blow Molding of Bulk Metallic Glass. *Journal of Microelectromechanical Systems*, **20**, 28-36. <https://doi.org/10.1109/JMEMS.2010.2090495>
- [60] Kumar, G., Tang, H.X. and Schroers, J. (2009) Nanomoulding with Amorphous Metals. *Nature*, **457**, 868-872. <https://doi.org/10.1038/nature07718>
- [61] Schroers, J. (2005) The Superplastic Forming of Bulk Metallic Glasses. *JOM*, **57**, 35-39. <https://doi.org/10.1007/s11837-005-0093-2>
- [62] Wang, Q., *et al.* (2014) Superior Tensile Ductility in Bulk Metallic Glass with Gradient Amorphous Structure. *Scientific Reports*, **4**, Article No. 4757.
- [63] Ferry, M., *et al.* (2013) Recent Developments in Ductile Bulk Metallic Glass Com-

- posites. *MRS Communications*, **3**, 1-12. <https://doi.org/10.1557/mrc.2012.32>
- [64] Ritchie, R.O. (2008) The Quest for Stronger, Tougher Materials. *Science*, **320**, 448. <https://doi.org/10.1126/science.320.5875.448a>
- [65] Nishiyama, N., *et al.* (2012) The World's Biggest Glassy Alloy Ever Made. *Intermetallics*, **30**, 19-24. <https://doi.org/10.1016/j.intermet.2012.03.020>
- [66] Hyers Robert, W. and Rogers Jan, R. (2008) A Review of Electrostatic Levitation for Materials Research. *High Temperature Materials and Processes*, **27**, 461-474.
- [67] Paradis, P.-F., *et al.* (2014) Materials Properties Measurements and Particle Beam Interactions Studies using Electrostatic Levitation. *Materials Science and Engineering: R. Reports*, **76**, 1-53. <https://doi.org/10.1016/j.mser.2013.12.001>
- [68] Guo, G.-Q., *et al.* (2015) How Can Synchrotron Radiation Techniques Be Applied for Detecting Microstructures in Amorphous Alloys? *Metals*, **5**, 2048-2057. <https://doi.org/10.3390/met5042048>
- [69] Guo, G.-Q., *et al.* (2015) Detecting Structural Features in Metallic Glass via Synchrotron Radiation Experiments Combined with Simulations. *Metals*, **5**, 2093-2108. <https://doi.org/10.3390/met5042093>
- [70] Michalik, S., *et al.* (2014) Structural Modifications of Swift-Ion-Bombarded Metallic Glasses Studied by High-Energy X-Ray Synchrotron Radiation. *Acta Materialia*, **80**, 309-316. <https://doi.org/10.1016/j.actamat.2014.07.072>
- [71] Gilman, J.J. (1975) Mechanical Behavior of Metallic Glasses. *Journal of Applied Physics*, **46**, 1625-1633. <https://doi.org/10.1063/1.321764>
- [72] Gandin, C.-A., Rappaz, M. and Tintillier, R. (1993) Three-Dimensional Probabilistic Simulation of Solidification Grain Structures: Application to Superalloy Precision Castings. *Metallurgical Transactions A*, **24**, 467-479. <https://doi.org/10.1007/BF02657334>
- [73] Heine, R.W., Loper, C.R. and Rosenthal, P.C. (1967) Principles of Metal Casting. McGraw-Hill, New York.
- [74] Kelly, P.M. and Zhang, M.-X. (2006) Edge-to-Edge Matching—The Fundamentals. *Metallurgical and Materials Transactions A*, **37**, 833-839. <https://doi.org/10.1007/s11661-006-0056-4>
- [75] Zhang, M.X. and Kelly, P.M. (2005) Edge-to-Edge Matching Model for Predicting Orientation Relationships and Habit Planes—The Improvements. *Scripta Materialia*, **52**, 963-968. <https://doi.org/10.1016/j.scriptamat.2005.01.040>
- [76] Taylor, H.F., Flemings, M.C. and Wulff, J. (1962) Foundry Engineering. John Wiley and Sons, Hoboken.
- [77] Rafique, M.M.A. and Iqbal, J. (2009) Modeling and Simulation of Heat Transfer Phenomena during Investment Casting. *International Journal of Heat and Mass Transfer*, **52**, 2132-2139. <https://doi.org/10.1016/j.ijheatmasstransfer.2008.11.007>
- [78] Bergman, T.L., Lavine, A.S. and Incropera, F.P. (2011) Fundamentals of Heat and Mass Transfer. 7th Edition, John Wiley & Sons, Incorporated, Hoboken.
- [79] Poirier, D.R. and Poirier, E.J. (1998) Heat Transfer Fundamentals for Metal Casting, with SI Units. Wiley, Hoboken.
- [80] Gao, W.H., *et al.* (2014) Martensite Structure and Phase Transformation of Quaternary ZrCuAlCo High Temperature Shape Memory Alloys. *Journal of Alloys and Compounds*, **607**, 99-103. <https://doi.org/10.1016/j.jallcom.2014.04.061>
- [81] Gao, W.-H., *et al.* (2015) Effects of Co and Al Addition on Martensitic Transformation and Microstructure in ZrCu-Based Shape Memory Alloys. *Transactions of*

- Nonferrous Metals Society of China*, **25**, 850-855.  
[https://doi.org/10.1016/S1003-6326\(15\)63673-1](https://doi.org/10.1016/S1003-6326(15)63673-1)
- [82] Soubeyroux, J.L., Pelletier, J.M. and Perrier de la Bâthie, R. (2000) *In Situ* Crystallization of Zirconium-Based Bulk Metallic Glasses. *Physica B: Condensed Matter*, **276-278**, 905-906. [https://doi.org/10.1016/S0921-4526\(99\)01585-9](https://doi.org/10.1016/S0921-4526(99)01585-9)
- [83] Zhou, W., Weng, W.P. and Hou, J.X. (2016) Glass-Forming Ability and Corrosion Resistance of ZrCuAlCo Bulk Metallic Glass. *Journal of Materials Science & Technology*, **32**, 349-354. <https://doi.org/10.1016/j.jmst.2015.12.012>
- [84] Li, Y., *et al.* (2012) Effects of Cu, Fe and Co Addition on the Glass-Forming Ability and Mechanical Properties of Zr-Al-Ni Bulk Metallic Glasses. *Science China Physics, Mechanics and Astronomy*, **55**, 2367-2371.  
<https://doi.org/10.1007/s11433-012-4919-y>
- [85] Hua, N., *et al.* (2011) Ni- and Cu-Free Zr-Al-Co-Ag Bulk Metallic Glasses with Superior Glass-Forming Ability. *Journal of Materials Research*, **26**, 539-546.  
<https://doi.org/10.1557/jmr.2010.65>
- [86] (2017) Private Communication with Dr. Daniel East (CSIRO).
- [87] Hofmann, D.C. and Johnson, W.C. (2011) Bulk Metallic Glass Matrix Composites. Google Patents.
- [88] Fu, X.L., Li, Y. and Schuh, C.A. (2005) Contributions to the Homogeneous Plastic Flow of *in Situ* Metallic Glass Matrix Composites. *Applied Physics Letters*, **87**, Article ID: 241904. <https://doi.org/10.1063/1.2140477>
- [89] Wu, F.-F., *et al.* (2014) Bulk Metallic Glass Composite with Good Tensile Ductility, High Strength and Large Elastic Strain Limit. *Scientific Reports*, **4**, Article No. 5302.
- [90] Pekarskaya, E., Kim, C.P. and Johnson, W.L. (2011) *In Situ* Transmission Electron Microscopy Studies of Shear Bands in a Bulk Metallic Glass Based Composite. *Journal of Materials Research*, **16**, 2513-2518.  
<https://doi.org/10.1557/JMR.2001.0344>
- [91] Wei, S., *et al.* (2013) Liquid-Liquid Transition in a Strong Bulk Metallic Glass-Forming Liquid. *Nature Communications*, **4**, Article No. 2083.  
<https://doi.org/10.1038/ncomms3083>
- [92] Xu, W., *et al.* (2015) Evidence of Liquid-Liquid Transition in Glass-Forming La<sub>50</sub>Al<sub>35</sub>Ni<sub>15</sub> Melt above Liquidus Temperature. *Nature Communications*, **6**, 7696.  
<https://doi.org/10.1038/ncomms8696>
- [93] Park, B.J., *et al.* (2006) Phase Separating Bulk Metallic Glass: A Hierarchical Composite. *Physical Review Letters*, **96**, Article ID: 245503.  
<https://doi.org/10.1103/PhysRevLett.96.245503>
- [94] Oh, J.C., *et al.* (2005) Phase Separation in Cu<sub>43</sub>Zr<sub>43</sub>Al<sub>7</sub>Ag<sub>7</sub> Bulk Metallic Glass. *Scripta Materialia*, **53**, 165-169. <https://doi.org/10.1016/j.scriptamat.2005.03.046>
- [95] Park, J.M., *et al.* (2012) Designing Zr-Cu-Co-Al Bulk Metallic Glasses with Phase Separation Mediated Plasticity. *Metallurgical and Materials Transactions A*, **43**, 2598-2603. <https://doi.org/10.1007/s11661-011-1050-z>
- [96] Jiang, F., *et al.* (2007) Microstructure Evolution and Mechanical Properties of Cu<sub>46</sub>Zr<sub>47</sub>Al<sub>7</sub> Bulk Metallic Glass Composite Containing CuZr Crystallizing Phases. *Materials Science and Engineering: A*, **467**, 139-145.  
<https://doi.org/10.1016/j.msea.2007.02.093>
- [97] Liu, J., *et al.* (2011) *In Situ* Spherical B2 CuZr Phase Reinforced ZrCuNiAlNb Bulk Metallic Glass Matrix Composite. *Journal of Materials Research*, **25**, 1159-1163.  
<https://doi.org/10.1557/JMR.2010.0138>

- 
- [98] Deng, J.W., *et al.* (2013) Nanometer to Micrometer Scaled Inhomogeneous Etching of Bulk Metallic Glasses by Ion Sputtering. *Intermetallics*, **34**, 75-82.  
<https://doi.org/10.1016/j.intermet.2012.11.007>
- [99] Gebert, A., Gostin, P. and Schultz, L. (2010) Effect of Surface Finishing of a Zr-Based Bulk Metallic Glass on Its Corrosion Behaviour. *Corrosion Science*, **52**, 1711-1720. <https://doi.org/10.1016/j.corsci.2010.01.027>
- [100] Abe, H., *et al.* (2009) Dealloying of Cu-Zr-Ti Bulk Metallic Glass in Hydrofluoric Acid Solution. *Materials Transactions*, **50**, 1255-1258.  
<https://doi.org/10.2320/matertrans.ME200823>
- [101] Pan, X.F., *et al.* (2011) Vickers Hardness and Compressive Properties of Bulk Metallic Glasses and Nanostructure-Dendrite Composites. *Journal of Materials Research*, **20**, 2632-2638. <https://doi.org/10.1557/JMR.2005.0328>
- [102] Bei, H., Xie, S. and George, E.P. (2006) Softening Caused by Profuse Shear Banding in a Bulk Metallic Glass. *Physical Review Letters*, **96**, Article ID: 105503.  
<https://doi.org/10.1103/PhysRevLett.96.105503>
- [103] Yoo, B.-G., *et al.* (2011) Role of Free Volume in Strain Softening of As-Cast and Annealed Bulk Metallic Glass. *Journal of Materials Research*, **24**, 1405-1416.  
<https://doi.org/10.1557/jmr.2009.0167>
- [104] Jiang, W.H., *et al.* (2011) Strain-Rate Dependence of Hardening and Softening in Compression of a Bulk-Metallic Glass. *Journal of Materials Research*, **22**, 2655-2658.  
<https://doi.org/10.1557/JMR.2007.0351>